PHYSICAL REVIEW B **69**, 245305 (2004)

Influence of conduction-band nonparabolicity on electron confinement and effective mass in $GaN_xAs_{1-x}/GaAs$ quantum wells

Stanko Tomić*
Computational Science and Engineering Department, CCLRC Daresbury Laboratory, Warrington, Cheshire WA4 4AD, United Kingdom

Eoin P. O'Reilly†
NMRC, University College, Lee Maltings, Prospect Row, Cork, Ireland

Peter J. Klar,‡ Heiko Grüning, and Wolfram Heimbrodt
Department of Physics and Material Sciences Center, Philipps-University, Renthof 5, D-35032 Marburg, Germany

Weimin M. Chen and Irina A. Buyanova
Department of Physics and Measurement Technology, Linköping University, Sweden
(Received 28 November 2003; published 9 June 2004)

We derive an analytical model to describe the conduction-band states of GaNAs-based quantum well structures, including the band anticrossing effect between *N* resonant states and the conduction-band edge. The predictions of the model are compared to those obtained using a full ten-band $\mathbf{k}\cdot\mathbf{p}$ model based on the same set of parameters. Both methods are then tested by comparison with the experimentally determined ground- and excited-state interband transition energies of GaN_xAs_{1-x} quantum wells of different well widths and *N* composition x obtained at 300 K and under hydrostatic pressures up to 2.0 GPa. We show that the transition energies can be described by a consistent set of material parameters in all the samples studied, and present how the conduction to valence-band offset ratio varies strongly with x in $GaN_xAs_{1-x}/GaAs$ quantum well structures. We conclude that the model presented can be used to predict the transition energies and electron subband structure of any $GaN_xAs_{1-x}/GaAs$ quantum well with well width between 2 and 25 nm, and *N* composition x between 1 and 4%, although further work is still required to confirm the optimum choice for the variation of band offset ratio with composition.

DOI: 10.1103/PhysRevB.69.245305 PACS number(s): 71.20.Nr, 73.21.Fg, 78.66.Fd, 62.50.+p

I. INTRODUCTION

Although the energy gap of GaAs is 1.52 eV at low temperature, and that of GaN is over 3 eV, when a small amount of arsenic is replaced by nitrogen in GaAs the energy gap initially decreases rapidly, by over 150 meV per % of *N*.[1–8]This extreme band-gap bowing is markedly different to conventional III-V alloys and has led to considerable interest and investigation of its origin. A major breakthrough in understanding was achieved with the demonstration by Shan *et al.* that the reduction in energy gap is due to a band anticrossing interaction (BAC) between the conduction-band edge and a higher-lying band of localized nitrogen resonant states.[9] Their model is consistent with a wide range of experimental data, but was not initially supported by a number of theoretical studies which used the pseudopotential method to carry out a detailed investigation of the lower-lying conduction-band states in ordered and disordered GaNAs supercells.[10,11] Theoretical studies based on the tight-binding (TB) method generally support the BAC model.[12–15] Because it uses a basis of localized orbitals, the TB method can provide significant insight into the influence of localized perturbations on the electronic structure, including the derivation of a modified $\mathbf{k}\cdot\mathbf{p}$ model to describe the band-edge dispersion in GaNAs and related alloys.[14]

Considerable insight can be gained into the conduction-band (CB) structure of conventional semiconductor quantum well (QW) structures using a one-band effective mass model to derive simple analytical expressions for confined state energies and in-plane effective mass. We derive here equivalent simple expressions based on the two-band BAC model for GaNAs heterostructures. The model gives results which we show by comparison with a full 10-band $\mathbf{k}\cdot\mathbf{p}$ model, Ref. 16, describe well the calculated variation of these properties in GaNAs.

We overview the consequences of the two-band model for GaNAs/GaAs QW's. The two-band model includes the strong nonparabolicity in the CB dispersion, leading to more confined states at a given well width than would be predicted using a one-band model. The in-plane effective mass also increases rapidly with increasing confinement energy, as expected from previous analysis. More surprisingly, electrons are predicted to be more strongly confined in narrow GaNAs/GaAs QW's than in equivalent GaAs/AlGaAs or GaInAs/GaAs QW's. Analysis of GaAs/AlGaAs and GaInAs/GaAs QWs typically finds increasing wave function penetration into the barrier as the well width decreases below about 5 nm.[17,18] The BAC interaction leads to reduced wave function penetration into the barrier in GaNAs/GaAs, with the ground-state electron level remaining localized in the well to narrower well widths.

We compare our model with experimental transition energy data in a wide range of GaNAs/GaAs QW's from which we derive a consistent (but not unique) set of material pa-

 ©2004 The American Physical Society

rameters, which are then suitable for describing the band offsets, confinement energies and in-plane effective masses of the conduction subbands of any $GaN_xAs_{1-x}/GaAs$ QW with a well width between 2 and 25 nm, and N content x between 1 and 4%.

The analytical model is derived and analyzed in the following section. We consider the best choice of material parameters in Sec. III, and compare the theoretical model with experiment in Sec. IV. Finally we present our conclusions in Sec. V.

II. DERIVATION OF ANALYTICAL MODEL

A. Band structure

To derive the analytical model, it is sufficient to account for the band anticrossing effect of the N levels with the conduction-band states and treat the valence band separately. The variation of the conduction-band dispersion with wave vector $\mathbf{k}$ in bulk GaN_xAs_{1-x} is given in the BAC model by finding the lower eigenvalue $E_-(k)$ of the Hamiltonian $H(x)$ linking two interacting energy levels

$$H(x) = \begin{pmatrix} E_N + ak^2 & V_{Nc} \\ V_{Nc} & E_c + bk^2 \end{pmatrix} \quad (1)$$

with the zone-center state at energy E_c associated with the extended conduction band-edge states of the GaAs matrix, and E_N the energy of the localized N resonant impurity states, with the two types of states linked by a matrix element V_{Nc} describing the interaction between them. The band dispersion is introduced via the two diagonal terms involving a and b, with $b = \hbar^2/2m_0 m_c^*$, where m_c^* is an appropriately chosen conduction-band edge effective mass for the host matrix, and a (usually set to zero) describes the dispersion of the nitrogen resonant band. We note that the band-edge effective mass in bulk GaN_xAs_{1-x} [given by the variation of the lower eigenvalue E_- of Eq. (1) with k] is larger than the host matrix effective mass m_c^*. We refer to this band-edge mass below as m_-^*, with the alloy conduction-band dispersion then given for small k as

$$E_-(k) = E_- + \frac{\hbar^2 k^2}{2m_0 m_-^*}. \quad (2)$$

We discuss the relation between m_c^* and m_-^* in more detail below.

The conduction-band dispersion as presented in Eqs. (1) and (2) is isotropic, with the effective mass m_c^* independent of the direction of the wave vector k. This assumption is appropriate for unstrained bulk semiconductors, and to carry out the derivation presented in this section. We will consider in later sections strained GaN_xAs_{1-x} layers grown on GaAs. The band dispersion then becomes anisotropic,[19] with different effective mass values required in Eq. (1) [Eq. (2)] within the growth plane, $m_{c\parallel}^*[m_{-\parallel}^*]$ and along the growth direction, $m_{c\perp}^*[m_{-\perp}^*]$.

We assume when considering GaN_xAs_{1-x} QW's grown pseudomorphically on GaAs that E_N and E_c vary with composition x and hydrostatic pressure p as

$$E_N = E_{N0} - (\gamma - \kappa)x + 2a_N(1 - c_{12}/c_{11})\varepsilon_{xx} + (dE_N/dp)p, \quad (3)$$

$$E_c = E_{c0} - (\alpha - \kappa)x + 2a_c(1 - c_{12}/c_{11})\varepsilon_{xx} + (dE_c/dp)p. \quad (4)$$

The linear shifts $(\alpha-\kappa)x$ and $(\gamma-\kappa)x$ account for conventional alloying effects, while the interaction matrix element $V_{Nc} = \beta\sqrt{x}$ reflects the composition dependence of the level repulsion effect. Although the terms involving κx are redundant in Eqs. (3) and (4), we include them here, as they are used later to describe the variation of the valence-band offset with composition. The two-level Hamiltonian of Eq. (1) remains valid in the GaAs barrier layers, where the resonant level and conduction-band edge are decoupled with $V_{Nc}=0$. The summand $2a_{N(c)}(1-c_{12}/c_{11})\varepsilon_{xx}$ accounts for the shift of the nitrogen (conduction) band due to the hydrostatic component of strain, e.g., in GaNAs QW layers, where $a_{N(c)}$ are the hydrostatic deformation potentials, c_{11} and c_{12} the elastic constants, and ε_{xx} is the in-plane strain due to the lattice mismatch with respect to the GaAs substrate. The summands $(dE_c/dp)p$ and $(dE_N/dp)p$ describe the shifts of the conduction-band edge and the N level under hydrostatic pressure. The BAC effect describes the coupling of those two bands in the well region, leading to two mixed states, the lower of which is at energy

$$E_- = \frac{E_N + E_c}{2} - \frac{1}{2}\sqrt{(E_N - E_c)^2 + 4V_{Nc}^2}. \quad (5)$$

We use Eq. (1) to determine an analytical expression for the zone center ($k_\parallel = 0$) confined state energies E_i in a GaNAs QW structure, centered at the origin and of width $2L$. We derive the expression here for even states. To find the allowed solutions we initially assume that the parameter a is small and positive, solve Schrödinger's equation in the well and in the barrier, and then apply appropriate boundary conditions at the well-barrier interface. [We set $a=0$ at the end of the derivation, as in previous calculations[20–22].] We can solve Eq. (1) to find two states at energy E within the well, one of which (k_{z-}) is a propagating and the other (k_{z+}) an evanescent state, with wave vectors $k_{z\pm}^2$ along the z (growth) direction. The general even two-component solutions of Schrödinger's equation, $\Psi^{(w)}(z)$, are then given within the well ($|z| < L$) by

$$\Psi^{(w)}(z) = B_1 \begin{pmatrix} \alpha_{N-} \\ \alpha_{c-} \end{pmatrix} \cos(k_{z-}z) + B_2 \begin{pmatrix} \alpha_{N+} \\ \alpha_{c+} \end{pmatrix} \cosh(k_{z+}z), \quad (6)$$

where $\alpha_{N(c)\pm}$ describes the amplitudes of the states projected onto the nitrogen resonant state (unperturbed conduction band-edge state), with $|\alpha_{N\pm}|^2 + |\alpha_{c\pm}|^2 = 1$.

Turning to the barrier (where $E_c = E_{c0}$ at ambient pressure), to ensure wave function matching across the interface, we include a resonant state at energy E_N above the conduction-band edge, and set $V_{Nc}=0$, as this state does not interact with the conduction-band edge. This resonant state plays no part in determining the confined state energy and wave functions, but is formally required to solve the enve-

lope function equation. Because the resonant and conduction-band edge states are decoupled in the barrier, the evanescently decaying barrier wave function $\Psi^{(b)}(z)$, required to match the well solution is given in the right-hand barrier $(z>L)$ by

$$\Psi^{(b)}(z)=C_1\begin{pmatrix}0\\1\end{pmatrix}\exp(-\kappa_{z-}z)+C_2\begin{pmatrix}1\\0\end{pmatrix}\exp(-\kappa_{z+}z), \quad (7)$$

where $b\kappa_{z-}^2=E_c-E$ and $a\kappa_{z+}^2=E_N-E$, respectively.

The allowed solutions of Eq. (1) must then satisfy appropriate boundary conditions across the interface (at $z=L$), namely, that

$$\Psi^{(w)}(z=L)=\Psi^{(b)}(z=L) \quad (8)$$

and also that

$$\begin{pmatrix}a & 0\\0 & b\end{pmatrix}\frac{d\Psi(z)}{dz} \quad (9)$$

is continuous across the interface.[26] We have four unknown quantities in Eqs. (6) and (7), and from Eqs. (8) and (9) four boundary conditions for even solutions of the envelope-function equation, through which we can derive a 4×4 determinant which must be satisfied for allowed even solutions, as described in Appendix A. We show there that as $a\rightarrow0$, the coefficients B_2 and C_2 also $\rightarrow0$, and we require only that the conduction-band component of the envelope function and b times its derivative are continuous, where $b\propto m_{cw}^{*-1}$ in the well, and $\propto m_{cb}^{*-1}$ in the barrier. This leads to an expression for the confined state energy very similar to that for the conventional one-band effective mass model:

$$\frac{k_{z-}}{m_{cw}^*}\tan(k_{z-}L)=\frac{\kappa_{z-}}{m_{cb}^*}. \quad (10)$$

The relationship between energy E and wave vector k_{z-} in the well can be determined by solving the 2×2 Hamiltonian of Eq. (1), to give

$$bk_{z-}^2=\frac{V_{Nc}^2}{E_N-E}+E-E_c. \quad (11)$$

A similar expression to Eq. (10) can also be used for odd states, with $\tan(k_{z-}L)$ replaced by $-\cot(k_{z-}L)$.

To demonstrate the validity and usefulness of Eq. (10), Fig. 1 shows the calculated room-temperature variation of confined electron state energy as a function of well width, $2L$, in a $GaN_{0.02}As_{0.98}/GaAs$ QW structure. The zero of energy is taken at the GaAs valence-band edge. The dashed line shows the results calculated using the ten-band $\mathbf{k}\cdot\mathbf{p}$ Hamiltonian[16] we have previously used when fitting experimental transition energies in GaNAs/GaAs QW's;[23–25] the open circles are the results obtained using the full two-band Hamiltonian of Eq. (1), while the solid line shows the results calculated using the analytical model of Eq. (10). Further details of the parameters used in Fig. 1 are given in Sec. III, and summarized in Sec. IV. As expected, the analytical expression of Eq. (10) agrees exactly with the energy states calculated numerically using the two-band model of Eq. (1). They also provide an excellent estimate of the ground-state confinement energy and of several of the excited-state energies, but start to overestimate the ten-band excited state energies when they approach the GaAs conduction-band-edge energy (set at 1.42 eV in Fig. 1). This discrepancy at higher energy arises because the two-level model overestimates the conduction-band dispersion at larger wave vector k. A similar discrepancy is observed when comparing the one-band effective mass model with the results of eight-band $\mathbf{k}\cdot\mathbf{p}$ calculations in conventional semiconductor alloys.[26]

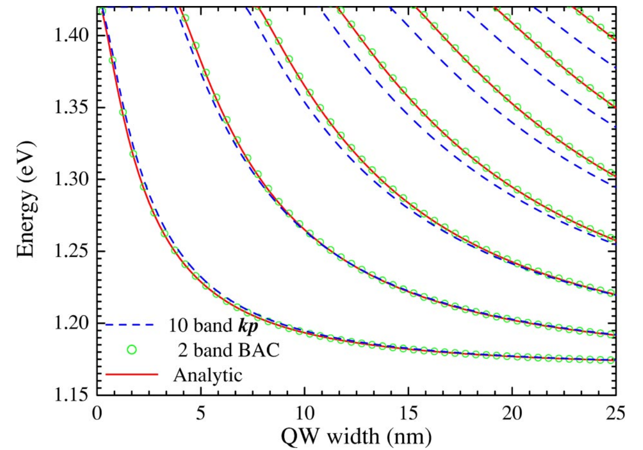

FIG. 1. (Color online) Well width dependence of the transition energies of $GaN_{0.02}As_{0.98}/GaAs$ quantum wells calculated by ten-band $\mathbf{k}\cdot\mathbf{p}$ Hamiltonian (dashed line), two-band BAC Hamiltonian (open circles) and Eq. (10) (solid line).

The analytical model of Eq. (10) provides a useful test of the convergence of the full numerical calculations. We used a plane-wave expansion method to determine the confined state energies in the GaNAs/GaAs QW calculations.[27] We find that the energy values converge more slowly than for conventional one-band or eight-band calculations. This is because the N component of the envelope function is discontinuous at the well/barrier interface, so that for the structures we considered at least twice as many plane waves were required to get converged energy levels compared to what is required for conventional alloys.

B. Effective masses

Having shown that the two-band model of Eq. (1) can give electron ground and excited state confinement energies in good agreement with more complete calculations using a ten-band $\mathbf{k}\cdot\mathbf{p}$ Hamiltonian, we now turn to use the two-band model to describe the electron effective mass in bulk GaNAs and within the plane of GaNAs/GaAs QW structures. The mixing between the N levels and the conduction-band edge reduces the band dispersion in GaN_xAs_{1-x} relative to the uncoupled band mass, with the inverse band edge mass, m_-^{*-1} given in the two-band Hamiltonian of Eq. (1) by

$$\frac{1}{m_-^*}=\frac{2m_0}{\hbar^2}(|\alpha_{c-}|^2b+|\alpha_{N-}|^2a). \quad (12)$$

Setting $a=0$ in Eq. (1) allows Eq. (12) to be simplified to

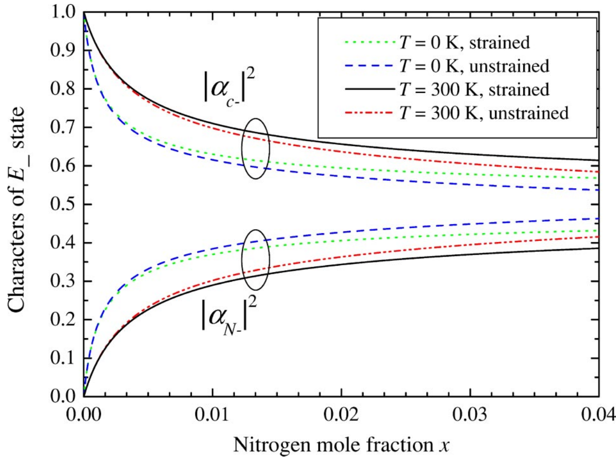

FIG. 2. (Color online) N dependence of the squared amplitude of the conduction-band character $|\alpha_{c-}|^2$ and of the N character $|\alpha_{N-}|^2$ at the band edge ($k_z=0$), of the mixed state E_- of bulk $GaN_{0.02}As_{0.98}$, at room and at low temperature, for unstrained structures, and for layers biaxially strained to the GaAs lattice constant.

$$m_-^* = \frac{m_c^*}{|\alpha_{c-}|^2}, \tag{13}$$

where $|\alpha_{c-}|^2$ was introduced in Eq. (6) and is given (at wave vector $k=k_z$) by

$$|\alpha_{c-}(k_z)|^2 = \frac{1}{2}\left(1 + \frac{E_N - E_c - bk_z^2}{\sqrt{[E_N - E_c - bk_z^2]^2 + 4V_{Nc}^2}}\right) \tag{14}$$

with $|\alpha_{N-}|^2 = 1 - |\alpha_{c-}|^2$ the corresponding composition-dependent squared amplitude of the nitrogen character of the given conduction-band state. Figure 2 depicts the band-edge ($k_z=0$) values of $|\alpha_{c-}|^2$ and $|\alpha_{N-}|^2$ for N contents $x \leqslant 0.04$, at room and low temperature, for unstrained bulk GaN_xAs_{1-x} and for strained GaN_xAs_{1-x} grown pseudomorphically on GaAs, all calculated using the parameters given in Tables I and II. It can be seen that the nitrogen character of the bulk band-edge state increases dramatically between $x=0$ and 0.01, reaching values of $|\alpha_{N-}|^2 \sim 0.40-0.45$ at larger x. This mixing is primarily responsible for the observed enhancement of the bulk effective mass in GaNAs.

Before deriving the electron effective mass in a GaNAs/GaAs QW structure, we first recall the calculation of the in-plane (parallel) effective mass, $m_\parallel^*$, for a conventional III-V QW structure. The in-plane band-edge effective mass $m_{\parallel i}^*$ for the ith confined state is given in the one-band model by[28,29]

$$\frac{1}{m_{\parallel i}^*} = \frac{P_i^{(w)}}{m_{cw\parallel}^*} + \frac{P_i^{(b)}}{m_{cb\parallel}^*}, \tag{15}$$

where $m_{cw\parallel}^*$ ($m_{cb\parallel}^*$) describes the in-plane conduction-band dispersion in the well (barrier) material. $P_i^{(w)}$ and $P_i^{(b)}=1-P_i^{(w)}$ are the probabilities of finding the ith confined state in the well and in the barrier respectively, with $P_i^{(w)}$ given by

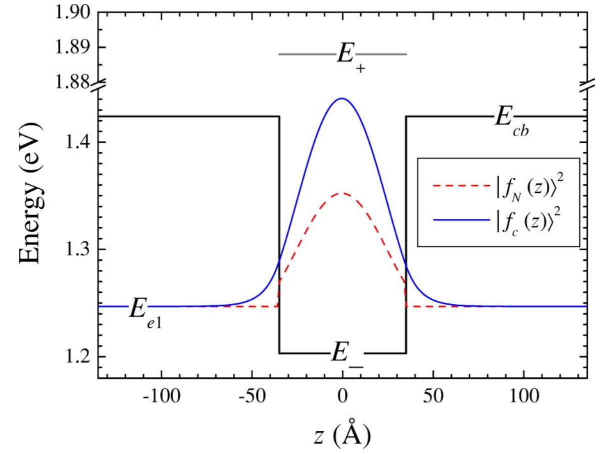

FIG. 3. (Color online) Conduction-band character $|f_c(z)\rangle^2$ (solid line) and nitrogen-band character $|f_N(z)\rangle^2$ (dashed line) of the first electron state in the conduction-band of a 7 nm wide $GaAs_{0.98}N_{0.02}$/GaAs quantum well.

$$P_i^{(w)} = \int_{-L}^{L} |\Psi_i(z)|^2 dz \tag{16}$$

for the normalized wave functions. The continuity of Ψ_i across the well/barrier boundary requires, using Eqs. (8) and (9) for the one-band model, that

$$B_1 \cos(k_w L) = C_1 \exp(-\kappa_b L) \tag{17}$$

for even states, where k_w and κ_b are the one-band analogues of k_{z-} and κ_{z-}, respectively. $P_1^{(w)}$ typically starts to decrease for the ground state band as the well width $2L$ drops below about 5 nm in a conventional QW. This is due both to a reduction in the integration range in Eq. (16), and also because the value of κ_b gets smaller in the barrier region, both of which effects lead to significant wave function penetration into the barrier.

The calculated wave function penetration and in-plane mass can be determined in the two-band model using first order perturbation theory, with the in-plane band-edge effective mass, $m_{-\parallel i}^*$ given by

$$\frac{1}{m_{-\parallel i}^*} = |\alpha_{c-}|^2 \frac{P_i^{(w)}}{m_{cw\parallel}^*} + \frac{P_i^{(b)}}{m_{cb\parallel}^*}, \tag{18}$$

where $m_{cw\parallel}^*$ here is the unperturbed conduction-band state in the well material [bottom right-hand term of Eq. (1)]. Equation (18) leads one to a markedly different behavior compared to Eq. (15). First, there is significantly less wave function penetration into the barrier. This arises because the boundary condition equivalent to Eq. (17) is given in the two-band model by

$$\alpha_{c-}(k_{z-}) B_1 \cos(k_{z-} L) = C_1 \exp(-\kappa_{z-} L) \tag{19}$$

and as $\alpha_{c-}(k_{z-})$ decreases with increasing confinement energy, due to the band anticrossing effects, so too will the relative magnitude of C_1. In other words, wave function matching only occurs with the conduction-band component of the well wave function, as illustrated in Fig. 3, which shows the calculated variation of the conduction band $|f_c(z)\rangle$

(solid line), and nitrogen state $|f_N(z)\rangle$ (dashed line) components of the ground-state envelope function in a 7 nm $GaN_{0.02}As_{0.98}/GaAs$ QW structure. As the confinement energy increases, the reduction in $\alpha_{c-}(k_{z-})$ tends both to reduce the wave function penetration into the barrier, and also to increase the average effective mass, $m^*_{-\|}$ within the well [see Eq. (13)]. Hence the zone-center effective mass, $m^*_{-\|i}$, tends to increase with decreasing well width, and also with increasing confinement energy (increasing i) for a fixed well width. A general expression describing how $P_i^{(w)}$ depends on wave vector k_z and well width $2L$ is given in Appendix B.

III. CHOICE OF PARAMETERS

A. Band structure

We describe in this section how we choose the material parameters to describe the conduction- and valence-band dispersion in bulk GaNAs and in GaNAs/GaAs QW structures at ambient pressure, and as a function of hydrostatic pressure. The heavy and light hole subband energies can be calculated by using a simple text-book one-dimensional QW model assuming that the unstrained valence band edge shifts as $E_v = E_{v0} + \kappa x$ in unstrained GaN_xAs_{1-x}, where E_{v0} is the valence-band edge of GaAs.

We use a linear variation κx for the dependence of the absolute chemical valence-band offset (VBO) on N content x in GaN_xAs_{1-x}. This is the simplest approach and is justified as the effect of N on the valence band is rather small compared to the strong red shift of the conduction-band edge at Γ and its bowing behavior as a function of x. This conduction-band bowing implies that, in a GaNAs/GaAs heterostructure, the electrons will be confined in the GaNAs layers. Whether the holes are also located in the GaNAs layers (i.e., the band alignment is type I) or in the GaAs layers (i.e., type II) is not *a priori* clear. Both possible band alignments were reported in the literature.[32–37,39] However, the current assembled experimental evidence strongly favours a type I band alignment for this heterosystem. The reported VBO's appear to vary considerably. The reasons are manifold. Two important points are (i) no clear distinction is made between the net VBO (including strain contributions) and the chemical VBO (corrected for strain contributions). (ii) Due to the nonlinearity of the GaN_xAs_{1-x} band gap the band offset ratio will vary with N composition x. We have previously estimated a chemical VBO ratio in the range of 15–30% in $GaN_{0.018}As_{0.982}/GaAs$ QW structures.[32] Krispin *et al.* reported a net VBO of only 5% for $GaN_{0.03}As_{0.97}/GaAs$ QW structures determined by capacitance-voltage measurements.[36,37] The value of $\kappa = 3.0$ eV that we use corresponds to a chemical VBO ratio of 30% for a $GaN_{0.018}As_{0.982}/GaAs$ QW structure. This choice of κ is in agreement with a type I band alignment. We have found that variation of κ between 1.5 and 3.0 eV does not affect the key results of this paper.

We assume a parabolic band dispersion for the heavy and light holes with effective masses $m^*_{hh} = (\gamma_1 - 2\gamma_2)^{-1}$ and $m^*_{lh} = (\gamma_1 + 2\gamma_2)^{-1}$ respectively.[26] (In practice, the light-hole mass depends on both strain and hydrostatic pressure; however we ignore this dependence in our analysis below, because the experimental photoreflectance data provide information predominantly on the heavy-hole confined states.) The biaxial strain in the layer leads to additional shifts of $2a_v(1 - c_{12}/c_{11})\varepsilon_{xx} + \varsigma$ for the heavy hole and $2a_v(1 - c_{12}/c_{11})\varepsilon_{xx} - [(\Delta_{so} + \varsigma) - \sqrt{9\varsigma^2 - 2\varsigma\Delta_{so} + \Delta_{so}^2}]/2$ for the light-hole band, respectively, where $\varsigma = b_{ax}(1 + 2c_{12}/c_{11})\varepsilon_{xx}$, and the valence-band deformation potentials are a_v and b_{ax}.[40] Hydrostatic pressure yields an additional shift $(dE_v/dp)p$. Combining the eigenenergies of the conduction and valence subbands yields the transition energies.

TABLE I. Relevant material parameters of the binary compounds GaAs and GaN ($T = 300$ K).

	GaAs[a]	GaN[b]
a_0(Å)	5.6533	4.50
E_g (eV)	1.424	
E_P (eV)	25.7	
m^*_c	0.0665	
c_{11} (GPa)	122.1	293
c_{12} (GPa)	56.6	159
a_c (eV)	−7.17	−6.71
a_v (eV)	1.16	0.69
b_{ax} (eV)	−2.0	−2.0
Δ_{so} (eV)	0.341	
$\gamma_1, \gamma_2, \gamma_3$	6.98, 2.06, 2.93	

[a]Reference 56.
[b]Reference 57.

The relevant material parameters of GaAs and GaN are given in Table I. If the values for both binaries are given, a linear interpolation was used for determining the value for GaN_xAs_{1-x}. The N related parameters specific to the model are given in Table II. They have been adjusted to obtain best agreement with the experimentally determined interband transitions, and are close to those predicted by tight-binding supercell calculations.[12–14]

We choose the parameters to describe the change in band structure with hydrostatic pressure as follows. The rate at which the band gap changes under hydrostatic pressure $(dE_g/dp) = (dE_c/dp) - (dE_v/dp)$ is a direct observable in the experiment, whereas, the individual rates for the conduction-band edge and the valence-band edge cannot be easily accessed by experiment. Theory relates (dE_g/dp) and the deformation potential $a_g = a_c - a_v$ via $(dE_g/dp) = -3a_g/(c_{11} + 2c_{12})$. Using the parameters given in Table I yields $(dE_g/dp) = 106$ meV/GPa for GaAs, which is close to our observed value of 116 meV/GPa. In the calculation we have

TABLE II. N related model parameters ($T = 300$ K).

N level		CB host		VB host	
E_{N0} (eV)	1.65	E_{c0} (eV)	1.424	E_{v0} (eV)	0.00
γ (eV)	3.00	α (eV)	1.55	κ (eV)	3.00
coupling parameter: $\beta = 2.45$(eV)					

chosen (dE_c/dp) and (dE_v/dp) such that their difference equals 116 meV/GPa and their ratio equals a_c/a_v as given in Table I. This yields values of $a_c=-7.83$ eV and $a_v=1.27$ eV. For the shift of the N related level we used $(dE_N/dp)=25$ meV/GPa, comparable to the observed pressure dependence of isolated N resonant levels in GaAs.[41,42] This leads to a value of the nitrogen level deformation potential of $a_N \approx a_v + 0.21(a_c - a_v) = -0.644 - 0.220x$ eV.

Finally, we acknowledge that the parameter fit presented here is not unique. Photoreflectance and photoluminescence excitation data have played a key role in determining the band offset ratio in conventional semiconductor alloys, such as GaAs/AlGaAs.[38] For such alloys, most of the key band structure parameters are known accurately from measurements on the bulk materials, and there is only one parameter, the valence-band offset (κ), which can be varied when fitting to the measured interband transition energies. This is not the case for dilute nitride alloys, where there still remains uncertainty in each of the parameters α, β, γ and κ in Table II. As a consequence, it is possible to vary κ over a relatively wide range (at least 1.5 eV $<\kappa<$ 3.0 eV), and by making minor adjustments to α, β, and γ still obtain a good fit to all of the experimental data presented in the following section. This does not negate the model presented here, but means that further work is still required to identify the best choice for the assumed variation of valence band offset with composition.

B. Two-band effective mass value

The conduction band effective mass m_c^* needed for the two-band Hamiltonian of Eq. (1) can be determined by direct diagonalization of the ten-band $\mathbf{k}\cdot\mathbf{p}$ Hamiltonian. The effective mass at the conduction-band edge is anisotropic in the ten-band model for bulk GaN_xAs_{1-x} strained pseudomorphically to the GaAs lattice constant. Extending previous eight-band $\mathbf{k}\cdot\mathbf{p}$ analysis[19] to the ten-band model, it can be shown that the bulk band edge mass $m_{-\perp}^*$ along k_z (perpendicular to the plane of the substrate) is given by

$$\frac{1}{m_{-\perp}^*} = |\alpha_{c-}|^2 \left[s + E_P \left(\frac{f_z}{E_- - E_{\text{lh}}} + \frac{1-f_z}{E_- - E_{\text{so}}} \right) \right] \tag{20}$$

while the mass in the growth plane, $m_{-\parallel}^*$, is given by

$$\frac{1}{m_{-\parallel}^*} = |\alpha_{c-}|^2 \left[s + \frac{E_P}{2} \left(\frac{1}{E_- - E_{\text{hh}}} + \frac{1-f_z}{E_- - E_{\text{lh}}} + \frac{f_z}{E_- - E_{\text{so}}} \right) \right] \tag{21}$$

where E_P is the energy related to the Kane interband transition matrix element $P_0 = -i(\hbar/m_0)\langle s|p_x|x\rangle$ with $E_P = 2m_0P_0^2/\hbar^2$; E_{hh}, E_{lh}, and E_{so} are the strained heavy-hole, light-hole and spin-orbit split-off band-edge energies, and s is a small parameter:

$$s = \frac{1}{m_c^*} - \frac{E_P}{3} \left(\frac{2}{E_g} + \frac{1}{E_g + \Delta_{\text{so}}} \right) \tag{22}$$

describing the influence of remote bands on the conduction-band edge effective mass. The parameter f_z is a measure of

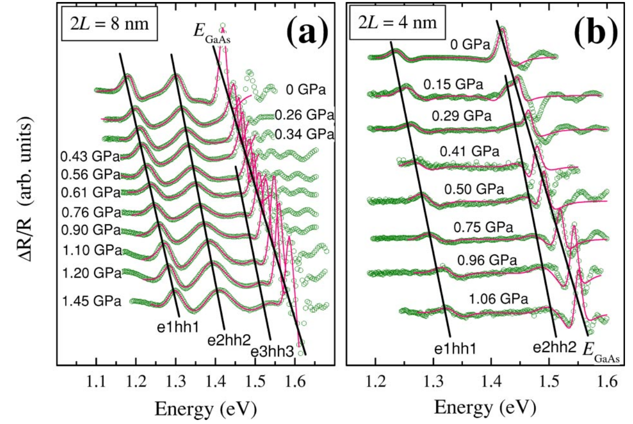

FIG. 4. (Color online) Series of photomodulated reflectance spectra of a 8 nm and a 4 nm $GaN_{0.018}As_{0.982}$/GaAs QW obtained under hydrostatic pressure at 300 K. The solid curves are fits to the experimental data (open circles). The straight lines are a guide to the eye and indicate the pressure shifts of the *eihhi* QW transitions and the GaAs barrier.

the fractional p_z-like character of the light-hole band. It is equal to 2/3 in an unstrained layer; and varies with shear strain as[30,31]

$$f_z = \frac{1}{2}\left(1 + \frac{\Delta_{\text{so}}/3 - 3\varsigma}{\sqrt{9\varsigma^2 - 2\varsigma\Delta_{\text{so}} + \Delta_{\text{so}}^2}} \right). \tag{23}$$

We can then define the unperturbed conduction-band edge dispersion in the lower right-hand term of Eq. (1) by

$$E_c(k) = E_c + \frac{\hbar^2}{2m_0|\alpha_{c-}|^2} \left(\frac{k_z^2}{m_{-\perp}^*} + \frac{k_\parallel^2}{m_{-\parallel}^*} \right) \tag{24}$$

with $m_{-\perp}^*$ and $m_{-\parallel}^*$ given by Eqs. (20) and (21), and $|\alpha_{c-}|^2$ by Eq. (14). This ensures the same (anisotropic) band edge mass in the two-band as in the ten-band model. We use Eq. (24) throughout this paper to define the two-band conduction-band edge effective mass, and so to ensure a fair comparison of the two-band and ten-band models. We include in Sec. IV B an analytical expression which gives an accurate fit of $m_{-\perp}^*$ and $m_{-\parallel}^*$ in Eq. (24) at room temperature.

IV. COMPARISON OF THEORY AND EXPERIMENT

A. Transition energies

We have tested the models presented in Sec. II by comparing calculated and experimental values of the transition energies of 21 GaN_xAs_{1-x}/GaAs QW's with well widths between 2 and 25 nm and $0.01<x<0.04$ grown by molecular-beam epitaxy (MBE) as well as by metal-organic vapor-phase epitaxy (MOVPE). The samples were studied by photomodulated reflectance (PR) spectroscopy at 300 K and under hydrostatic pressures up to 2.0 GPa. Experimental details as well as the extraction of the transition energies by fitting the spectra are described in detail elsewhere.[24,25,32]

Typical data are presented in Figs. 4(a) and 4(b), which show a series of PR spectra obtained under hydrostatic pressure at 300 K of two $GaN_{0.018}As_{0.982}$/GaAs QW's of width 8

and 4 nm, respectively. In the first series of spectra in Fig. 4(a) three signals can be clearly detected at all pressures; a fourth one can be discerned in the spectra for pressures exceeding 0.7 GPa. The signal at the highest energy originates from the GaAs barrier. The signals energetically below the barrier signal correspond to interband transitions between confined QW states. They are assigned to the three allowed transitions *eihhi* between the *i*th heavy-hole and *i*th electron QW subbands. No signals arising from interband transitions *eilhi* between light-hole subbands and electron subbands can be discerned in the spectra of this sample. However, this is typical of GaNAs/GaAs QW's when the corresponding transition energies are larger than that of $e1hh1$. The $e1lh1$ transition is observed only in the PR spectra if this transition is lowest in energy. This is the case for wider quantum wells where band shifts due to tensile strain in the GaNAs layer dominate quantum confinement effects for the lowest-energy transitions.[24,32]

In the second series of spectra in Fig. 4(b) two signals can be clearly seen at ambient pressure: the GaAs signal at 1.42 eV and the QW transition $e1hh1$ at approximately 1.25 eV. Both signals are shifting to higher energies with increasing pressure. The line shape of the GaAs barrier signal is changing dramatically in the pressure range between 0.15 and 0.29 GPa. This is due to an interference between the GaAs barrier signal and the signal of the $e2hh2$ QW transition. We calculate that the second electron state becomes confined in the QW in this pressure range, due to the increasing interaction between the nitrogen resonant state and the conduction-band edge as the value of E_N-E_c decreases with pressure. From a pressure of 0.5 GPa up to 1.1 GPa, the $e2hh2$ signal can be seen as a weak feature on the low-energy side of the GaAs signal in the corresponding PR spectra.

The PR spectra in Fig. 4(a) were fitted with three oscillators for pressures of less than 0.7 GPa and with four oscillators above 0.7 GPa. The PR spectra in Fig. 4(b) were fitted with two oscillators for pressures below 0.15 GPa and with three oscillators above 0.15 GPa. In both cases the fits agree very well with the measured PR data. The pressure dependence of the *eihhi* transitions is much smaller than that of the GaAs barrier and even decreases with increasing i for the 8 nm $GaN_{0.018}As_{0.982}/GaAs$ QW. The latter is strong experimental evidence that the electron effective mass varies for the different conduction-band subbands.

Figure 5 compares the experimentally determined transition energies of a series of $GaN_xAs_{1-x}/GaAs$ QW's of different width with those calculated using the ten-band $\mathbf{k}\cdot\mathbf{p}$ model and the analytical model of Eq. (10). The MBE grown samples (open circles) had a composition $x=0.016(\pm 0.001)$, while the MOVPE samples (solid circles) had $x=0.018(\pm 0.001)$. The theoretical fit was carried out using our material parameters for $x=0.017$. The agreement between experiment and the ten-band $\mathbf{k}\cdot\mathbf{p}$ calculation is very good throughout the series for all allowed transitions *eihhi*. The analytical model using the material parameters deduced from the ten-band $\mathbf{k}\cdot\mathbf{p}$ Hamiltonian gives excellent agreement with the full calculation and with experiment up to the $e3hh3$ transition. The differences between the models increase for higher QW transitions. This is to be expected: we have already seen in Fig. 1 how the two-band Hamiltonian of Eq. (1) underestimates the conduction-band nonparabolicity of GaNAs and hence overestimates slightly the confinement energy of the higher-lying conduction states, ei ($i>3$).

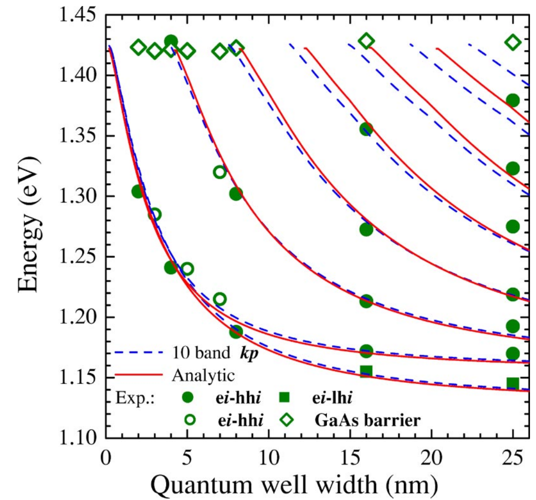

FIG. 5. (Color online) Comparison of transition energies in $GaN_{0.018}As_{0.982}/GaAs$ QW's of different width extracted from photomodulated reflectance spectra with those calculated using the ten-band $\mathbf{k}\cdot\mathbf{p}$ model (dashed lines) and the analytical model (solid lines). Ambient pressure and $T=300$ K.

Figure 6 compares the measured hydrostatic pressure dependence of the transition energies in a 9 nm $GaN_{0.013}As_{0.987}/GaAs$, a 8 nm $GaN_{0.018}As_{0.982}/GaAs$, and a 7 nm $GaN_{0.024}As_{0.976}/GaAs$ QW with those calculated in the framework of the ten-band $\mathbf{k}\cdot\mathbf{p}$ model and the analytical model. Again the agreement between experiment and both theories is very good. A similar quality of fit is obtained for all other samples using the material parameters given in Tables I and II. Using these parameters, we estimate (keeping terms linear in x) that the nitrogen level $E_N(x)$, and the conduction-band of the host material $E_c(x)$, vary with x as

$$E_N(x) \approx 1.65 - 0.141x, \tag{25}$$

$$E_c(x) \approx 1.424 - 0.264x, \tag{26}$$

while the conduction-band offset $\Delta E_c = E_c(\mathrm{GaAs}) - E_{-}(\mathrm{GaN}_x\mathrm{As}_{1-x})$ varies with x as

$$\Delta E_c(x) \approx -0.113 + 0.202x + \sqrt{0.013 + 6.016x} \tag{27}$$

the heavy-hole band offset $\Delta E_{\mathrm{hh}}(x)$ varies as

$$\Delta E_{\mathrm{hh}}(x) \approx 2.490x \tag{28}$$

and the light-hole offset $\Delta E_{\mathrm{lh}}(x)$ as

$$\Delta E_{\mathrm{lh}}(x) \approx 4.064x \tag{29}$$

as illustrated in Fig. 7. We note that because the conduction-band offset $\Delta E_c(x)$ has a strong nonlinear variation with x, the band offset ratios $\Delta E_c:\Delta E_{\mathrm{hh}}$ and $\Delta E_c:\Delta E_{\mathrm{lh}}$ vary strongly with x, with the calculated value of $\Delta E_c:\Delta E_{\mathrm{hh}}(\Delta E_c:\Delta E_{\mathrm{lh}})$ decreasing from 91:9 (87:13) for finite x approaching 0 to 80:20 (70:30) at $x=0.04$, respectively.

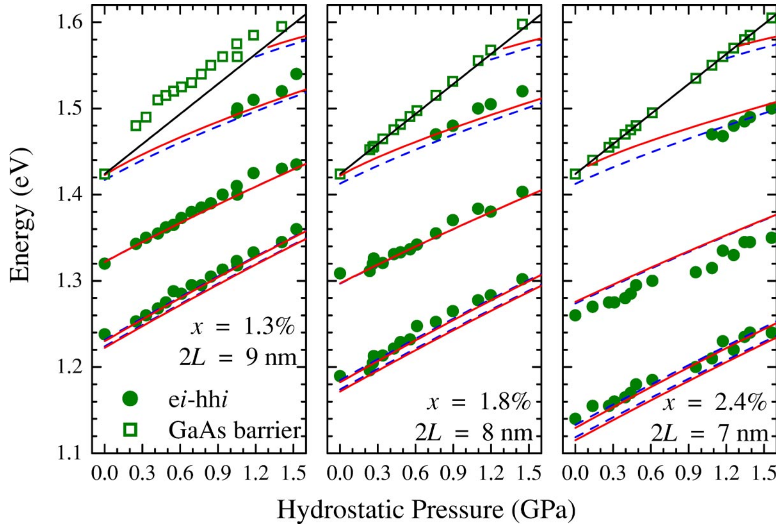

FIG. 6. (Color online) Comparison of the hydrostatic pressure dependence of the transition energies of 9 nm $GaN_{0.0133}As_{0.9887}/GaAs$, 8 nm $GaN_{0.018}As_{0.982}/GaAs$, and 7 nm $GaN_{0.024}As_{0.976}/GaAs$ QWs extracted from photomodulated reflectance spectra with those calculated in the framework of the ten-band $\mathbf{k}\cdot\mathbf{p}$ model (dashed lines) and the analytical model (solid lines) all at $T=300$ K.

B. Electron effective masses

The dashed lines in Fig. 8 show the calculated variation of $m^*_{-\perp}$ and $m^*_{-\|}$, respectively, as a function of x in bulk GaN_xAs_{1-x} grown pseudomorphically on GaAs, obtained from the ten-band $\mathbf{k}\cdot\mathbf{p}$ model. The room temperature strained electron effective mass is well fitted by an expression of the form

$$m^*_-(x) \approx 0.0665[1 - qx - r\Delta E_c(x)], \tag{30}$$

where $q=2.8382(1.3154)$ and $r=0.7773(0.7672)$ eV^{-1} for $m^*_{-\perp}(m^*_{-\|})$, as illustrated by the solid triangles in Fig. 8.

Figure 9 shows the calculated variation of the in-plane band-edge effective mass $m^*_{-\|i}$ as a function of QW width for two different nitrogen concentrations, $x=0.01$ and 0.02 and two temperatures, $T=4$ K and $T=300$ K, calculated by numerical differentiation of the band dispersion for the full ten-band model (dashed lines) and the two-band Hamiltonian of Eq. (1) (open circles), and also by direct application of the analytical two-band model of Eq. (18) (solid line). For the two-band model, we used the values of $m^*_{cw}=|\alpha_{c-}|^2\times m^*_{-\perp}$ when calculating the confined state energies using Eq. (10), while we used Eq. (18) when calculating the in-plane mass $m^*_{-\|i}$ of the ith subband in a GaNAs/GaAs QW structure. The overall agreement between the three models is good for the ground state in-plane effective mass; but the two-band nu-

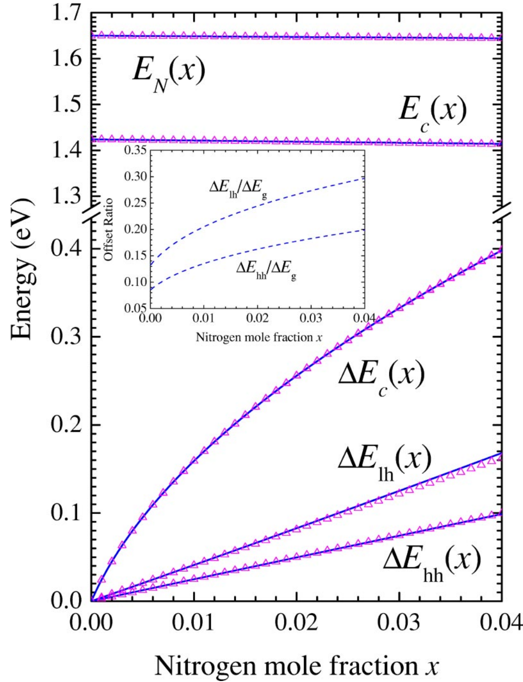

FIG. 7. (Color online) Calculated variation of the conduction, ΔE_c, heavy-hole ΔE_{hh} and light-hole ΔE_{lh} band offsets as well as nitrogen resonant level E_N and conduction-band edge of host material E_c, as a function of N composition, x, for a GaN_xAs_{1-x} layer grown pseudomorphically on GaAs. Solid lines present band offsets obtained numerically using parameters from Tables I and II, while the open triangles are obtained using the analytical expressions of Eqs. (25)–(29). Inset: dashed lines present the band offset ratios $\Delta E_{hh}/\Delta E_g$ and $\Delta E_{lh}/\Delta E_g$.

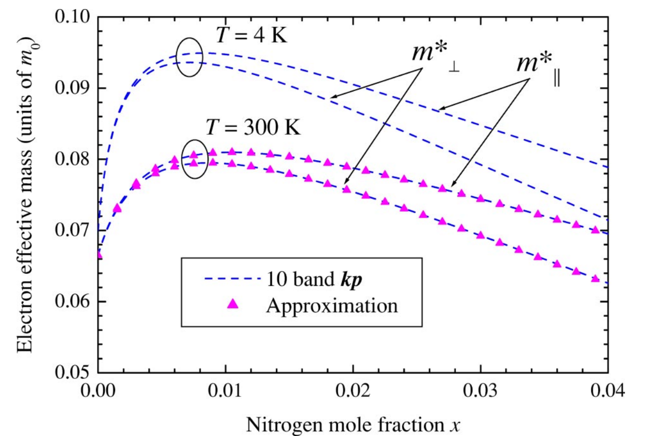

FIG. 8. (Color online) Calculated variation of the perpendicular and in-plane bulk conduction-band edge masses as a function of nitrogen concentration at low and room temperature. Dashed lines: obtained numerically using the ten-band $\mathbf{k}\cdot\mathbf{p}$ Hamiltonian; solid triangles: the room temperature mass values obtained using Eq. (30) in the two-band BAC model.

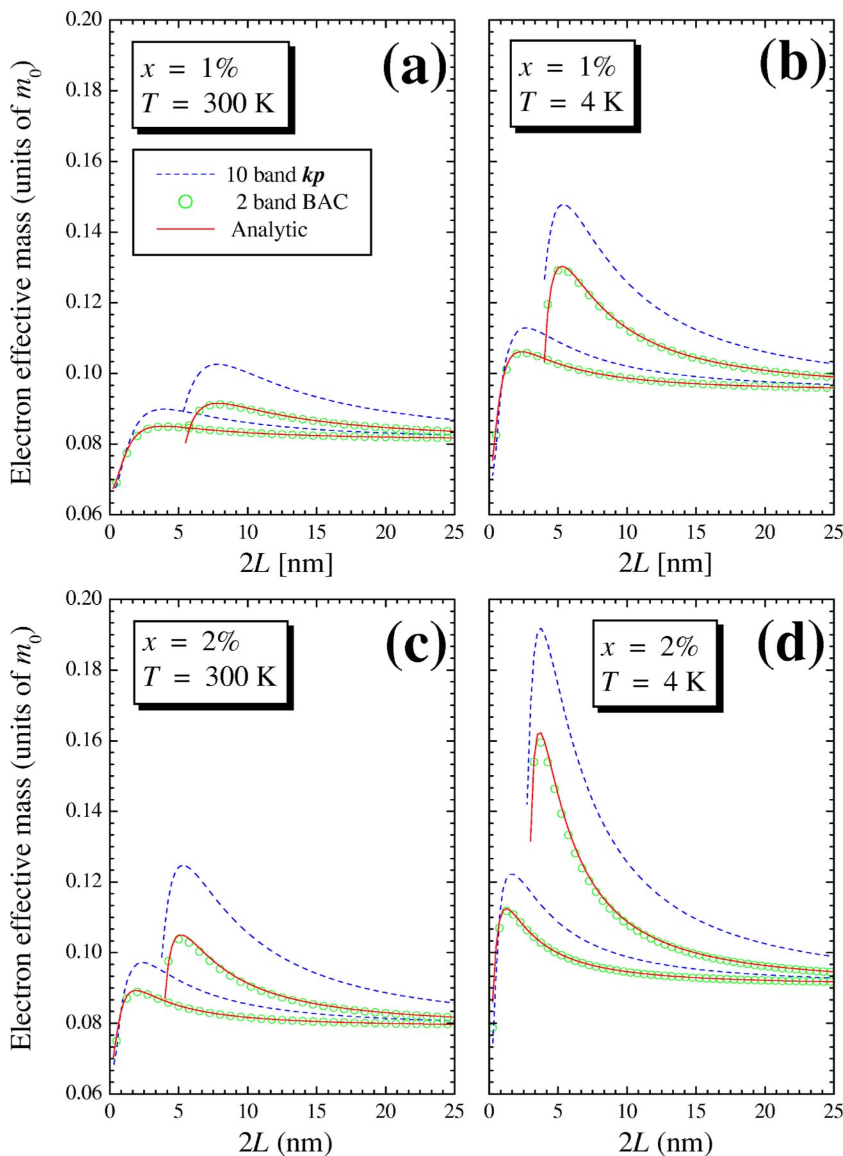

FIG. 9. (Color online) Calculated variation of in-plane effective mass of the CB ground and first excited QW states as a function of QW width $2L$ for $x=1\%$ and $x=2\%$ at low and room temperature. Dashed line: ten-band $\mathbf{k}\cdot\mathbf{p}$ Hamiltonian; open circles: numerical solution of two-band BAC model; solid line: analytical solution obtained using Eq. (18).

merical and analytical results start to underestimate the results of the full calculation for the higher confined levels. The minor discrepancies observed between the analytical and numerical two-band results arise because the numerical results are not fully converged, even when we include 201 plane waves to calculate the dispersion in a structure with total period 40 nm. All three models display similar trends as a function of well width: in wide wells, the effective mass approaches the bulk strained layer parallel mass of Fig. 8. Because of the strong conduction-band nonparabolicity in GaNAs, the mass tends to increase both as the confinement energy increases for a fixed well width, and also as the well width decreases for a given confined level. The peak in-plane mass occurs in relatively narrow wells ($2L=2-4$ nm) for the ground state and in slightly wider wells (5–8 nm) for the first excited state, with the calculated mass decreasing towards the GaAs value in narrower wells, due to wave function penetration into the barrier.

Our calculated variation of the band dispersion along the growth direction is consistent with the analysis of previous PR measurements at 300 K, where Wu *et al.* estimated a value of about $0.11m_0$ for the effective mass of $GaN_xAs_{1-x}/GaAs$ QW's with $1.2\% < x < 2.8\%$ and well width of less than 10 nm.[21] The room temperature band-edge masses calculated using the ten-band $\mathbf{k}\cdot\mathbf{p}$ Hamiltonian have provided a successful description of the gain characteristics in GaInNAs lasers,[23,44–46,52] while the two-band BAC model has also provided a successful description of the electron mass away from the band edge.[22] Although our calculated values for the in-plane mass show significant enhancement compared to GaAs, they generally underestimate the values obtained from low-temperature measurements which probe directly the conduction band-edge mass. Hai *et al.*[34,47] determined mass values of $0.12m_0$ and $0.19m_0$ at 4 K by optically detected cyclotron resonance on 7 nm $GaN_xAs_{1-x}/GaAs$ QW's with $x=1.2\%$ and 2.0%, respectively. Högersthal *et al.* determined a value of $0.15m_0$ for an epitaxial $GaN_{0.016}As_{0.984}$ layer at 5 K by magnetophotoluminescence.[48] In a similar experiment with low N concentration ($x \leqslant 0.5\%$), the same authors observe a small increase in effective mass to 0.074 for x as low as 0.043%, rising to a value of about 0.13 for $x > 0.1\%$.[49]

There are several possible causes for the discrepancy between our calculated room temperature masses and the experimental values. First, the mass values we calculate at 300 K are smaller than those determined at low-temperatures; with decreasing temperature the conduction-band edge approaches the N level and thus level repulsion effects increase, leading to an increasing effective electron mass. Also the value of effective mass derived from cyclotron resonance measurements[34,44] cannot be compared directly with the in-plane effective mass defined here. Previous analysis has shown how strong nonparabolicity introduces differences between the two values.[28,29,50] However neither of these factors appears sufficient to explain the observed mass values. We suggest that the most likely cause of the observed discrepancy is related to the presence of a small number of N related cluster states, which lie close in energy to the conduction-band minimum.[51] These cluster states are omitted in the two-level BAC model of Eq. (1). Although there are comparatively few cluster states, tight-binding calculations we have undertaken indicate that those cluster states which are close in energy to the conduction-band minimum can hybridize with the E_- state.[55] This hybridization may then reduce the conduction-band Γ character, $|\alpha_{c-}|^2$ at the band edge, thereby contributing to the experimentally observed increase in effective mass.

V. DISCUSSION AND CONCLUSIONS

A ten-band $\mathbf{k}\cdot\mathbf{p}$ Hamiltonian has previously been used to describe successfully the variation of ground state and excited-state confinement energy in Ga(In)NAs QW's as a function of QW width, N composition and hydrostatic pressure.[23,53] It has also been used to design the layer structure in GaInNAs/GaNAs/GaAs heterostructures. The calculated gain spectrum of 1.3 μm GaInNAs QW lasers was in excellent agreement with the measured gain spectrum,[48,49] thus allowing the model to be used to predict that the gain characteristics of 1.3 μm GaInNAs QW lasers will be comparable to or exceed those of InP-based 1.3 μm lasers.[45,46] Theoretical analysis based on the tight-binding method has justified this ten-band $\mathbf{k}\cdot\mathbf{p}$ model for bulk GaNAs but has not yet provided a rigorous derivation of how to apply the model to heterostructures, including the choice of appropriate boundary conditions across the heterointerface. We have applied the model here assuming a sharp interface between the GaNAs well and GaAs barrier. This assumption needs more careful consideration in a dilute alloy; only one in 50 As atoms is replaced by N in a 2% alloy. Nevertheless the application of our method to analyze PR data on a wide range of samples shows that the assumption of a sharp interface works well (even in 2 nm GaNAs layers), although it is clear that the true boundaries will not be so sharply defined. The strong disordering introduced by N will also weaken k selection in the alloy, so that the concepts of band dispersion and effective mass are not as well defined as in a conventional alloy.[54] Nevertheless our theoretical description of the zone-center confined state energies, and their pressure dependence across a wide range of samples shows that the dispersion calculated using either the ten-band or the two-band model is a useful concept along the growth direction in GaNAs/GaAs heterostructures. The calculated values of $m^*_{-\|}$ are enhanced compared to GaAs but still lower than those measured at low temperatures. Previous analysis has however confirmed the usefulness of the method for describing, e.g., the effective mass away from the band edge and also the gain characteristics of GaInNAs QW's. Further work is still required to underpin and fully justify the theoretical model but nevertheless the results presented here provide a useful approach to the design, modeling and physical investigations of Ga(In)NAs/GaAs heterostructures.

In summary, we have given an analytical model and a set of material parameters for predicting the transition energies and in-plane effective masses of the electron subbands of any $GaN_xAs_{1-x}/GaAs$ QW with well width between 2 and 25 nm and N composition x of 1–4%. This model can be readily modified to describe any GaInNAs-based QW's. Such models will be useful for the analysis and optimization of GaInNAs laser structures.

ACKNOWLEDGMENTS

We are very grateful for funding by the DFG (Germany), by Science Foundation Ireland, and by EPSRC (UK). We thank W. Stolz and J. Koch for growing the MOVPE samples, H.P. Xin and C.W. Tu for providing the MBE samples, and S. Healy for useful discussions. We thank the Interdisciplinary Research Center Optodynamics of the Philipps-University for support.

APPENDIX A

The 4×4 determinant which must be satisfied for allowed even solutions of Eq. (1) is given as

$$\begin{pmatrix} \alpha_{N-} & \alpha_{N+}\coth(k_{z+}L) & -1 & 0 \\ \alpha_{c-} & \alpha_{c+}\coth(k_{z+}L) & 0 & -1 \\ -\alpha_{N-}k_{z-}\tan(k_{z-}L) & \alpha_{N+}k_{z+} & \kappa_{z+} & 0 \\ -\alpha_{c-}b_w k_{z-}\tan(k_{z-}L) & \alpha_{c+}b_w k_{z+} & 0 & b_b\kappa_{z-} \end{pmatrix} \tag{A1}$$

while the corresponding secular equation is

$$\alpha_{N+}\alpha_{c-}[b_w k_{z-}\tan(k_{z-}L) - b_b\kappa_{z-}](k_{z+}+\kappa_{z+}) - \alpha_{N-}\alpha_{c+}[k_{z-}\tan(k_{z-}L) - \kappa_{z+}](b_w k_{z+} + b_b\kappa_{z-}) = 0, \tag{A2}$$

where we have let $\coth(\kappa_{z+}L)\to 1$ as $a\to 0$, and where

$$\alpha_{c+} = -\frac{aV_{Nc}}{b_w(E_N-E)+a(E_c-E)}\alpha_{N+}\to 0 \tag{A3}$$

if $a\to 0$. Equation (A2) then reduces to

$$b_w k_{z-}\tan(k_{z-}L) - b_b\kappa_{z-} = 0, \tag{A4}$$

which is identical to Eq. (10) in the main text.

APPENDIX B

In the frame of the BAC model, the probability of finding an electron from the ith confined state to be in the well, $P_i^{(w)}$, is given by

$$P_i^{(w)} = \frac{\sin(2k_{z-}L)/2k_{z-} + L}{|\alpha_{c-}|^2 \cos^2(k_{z-}L)/\kappa_{z-} + \sin(2k_{z-}L)/2k_{z-} + L} \quad \text{(B1)}$$

for even states and

$$P_i^{(w)} = \frac{-\sin(2k_{z-}L)/2k_{z-} + L}{|\alpha_{c-}|^2 \sin^2(k_{z-}L)/\kappa_{z-} - \sin(2k_{z-}L)/2k_{z-} + L} \quad \text{(B2)}$$

for odd states, where k_{z-} is defined in Eq. (11) of the main text.

*Electronic address: s.tomic@dl.ac.uk
†Electronic address: eoreilly@nmrc.ie
‡Electronic address: klarp@mailer.uni-marburg.de

[1] T. Makimoto, H. Saito, T. Nishida, and N. Kobayashi, Appl. Phys. Lett. **70**, 2984 (1997).
[2] M. Weyers, M. Sato, and H. Ando, Jpn. J. Appl. Phys., Part 2 **31**, L853 (1992).
[3] M. Kondow, K. Uomi, K. Hosomi, and T. Mozume, Jpn. J. Appl. Phys., Part 2 **33**, L1056 (1994).
[4] G. Pozina, I. Ivanov, B. Monemar, J. V. Thordson, and T. G. Andersson, J. Appl. Phys. **84**, 3830 (1998).
[5] W. G. Bi and C. W. Tu, Appl. Phys. Lett. **70**, 1609 (1997).
[6] H. Grüning, L. Chen, Th. Hartmann, P. J. Klar, W. Heimbrodt, F. Höhnsdorf, J. Koch, and W. Stolz, Phys. Status Solidi B **215**, 39 (1999).
[7] J. D. Perkins, A. Mascarenhas, Y. Zhang, J. F. Geisz, D. J. Friedman, J. M. Olson, and S. R. Kurtz, Phys. Rev. Lett. **82**, 3312 (1999).
[8] P. J. Klar, H. Grüning, W. Heimbrodt, J. Koch, F. Höhnsdorf, W. Stolz, P. M. A. Vicente, and J. Camassel, Appl. Phys. Lett. **76**, 3439 (2000).
[9] W. Shan, W. Walukiewicz, J. W. Ager, III, E. E. Haller, J. F. Geisz, D. J. Friedman, J. M. Olson, and S. R. Kurtz, Phys. Rev. Lett. **82**, 1221 (1999).
[10] E. D. Jones, N. A. Modine, A. A. Allerman, S. R. Kurtz, A. F. Wright, S. T. Tozer, and X. Wei, Phys. Rev. B **60**, 4430 (1999).
[11] T. Mattila, S. H. Wei, and A. Zunger, Phys. Rev. B **60**, R11245 (1999).
[12] A. Lindsay and E. P. O'Reilly, Solid State Commun. **112**, 443 (1999).
[13] A. Lindsay and E. P. O'Reilly, Solid State Commun. **118**, 313 (2001).
[14] E. P. O'Reilly, A. Lindsay, S. Tomić, and M. Kamal-Saadi, Semicond. Sci. Technol. **17**, 870 (2002).
[15] A. Lindsay and E. P. O'Reilly, Physica E (Amsterdam) (to be published).
[16] S. Tomić, E. P. O'Reilly, R. Fehse, S. J. Sweeney, A. R. Adams, A. D. Andreev, S. A. Choulis, T. J. C. Hosea, and H. Riechert, IEEE J. Sel. Top. Quantum Electron. **9**, 1228 (2003).
[17] R. L. Greene, K. K. Bajaj, and D. E. Phelps, Phys. Rev. B **29**, 1807 (1984).
[18] M. J. L. S. Haines, N. Ahmed, S. J. A. Adams, K. Mitchell, I. R. Agool, C. R. Pidgeon, B. C. Cavenett, E. P. O'Reilly, A. Ghiti, and M. T. Emeny, Phys. Rev. B **43**, 11 944 (1991).
[19] G. Hendorfer and J. Schneider, Semicond. Sci. Technol. **6**, 595 (1991).
[20] J. Hader, S. W. Koch, J. V. Moloney, and E. P. O'Reilly, Appl. Phys. Lett. **76**, 3685 (2000).
[21] J. Wu, W. Shan, W. Walukiewicz, K. M. Yu, J. W. Ager, III, E. E. Haller, H. P. Xin, and C. W. Tu, Phys. Rev. B **64**, 085320 (2001).
[22] C. Skierbiszewski, Semicond. Sci. Technol. **17**, 803 (2002).
[23] P. J. Klar, H. Grüning, W. Heimbrodt, G. Weiser, J. Koch, K. Volz, W. Stolz, S. W. Koch, S. Tomić, S. A. Choulis, T. J. C. Hosea, E. P. O'Reilly, M. Hofmann, J. Hader, and J. V. Moloney, Semicond. Sci. Technol. **17**, 830 (2002).
[24] H. Grüning, P. J. Klar, W. Heimbrodt, J. Koch, W. Stolz, A. Lindsay, S. Tomić, and E. P. O'Reilly, High Press. Res. **22**, 293 (2002).
[25] P. J. Klar, H. Grüning, W. Heimbrodt, J. Koch, W. Stolz, S. Tomić, and E. P. O'Reilly, Solid-State Electron. **47**, 437 (2002).
[26] A. T. Meney, B. Gönül, and E. P. O'Reilly, Phys. Rev. B **50**, 10 893 (1994).
[27] A. D. Andreev and E. P. O'Reilly, Phys. Rev. B **62**, 15 851 (2000); J. A. Barker and E. P. O'Reilly, *ibid.* **61**, 13 840 (2000).
[28] U. Ekenberg, Phys. Rev. B **36**, 6152 (1987).
[29] U. Ekenberg, Phys. Rev. B **40**, 7714 (1989).
[30] E. P. O'Reilly and A. R. Adams, IEEE J. Quantum Electron. **30**, 366 (1994).
[31] G. Jones and E. P. O'Reilly, IEEE J. Quantum Electron. **29**, 1344 (1993).
[32] P. J. Klar, H. Grüning, W. Heimbrodt, J. Koch, W. Stolz, P. M. A. Vicente, A. M. Kamal-Saadi, A. Lindsay, and E. P. O'Reilly, Phys. Status Solidi B **223**, 163 (2001).
[33] T. Kitatani, M. Kondow, T. Kikawa, Y. Yazawa, M. Okai and K. Uomi, Jpn. J. Appl. Phys., Part 1 **38**, 5003 (1999).
[34] I. A. Buyanova, G. Pozina, P. N. Hai, W. M. Chan, H. P. Xin, and C. W. Tu, Phys. Rev. B **63**, Art.No. 033303 (2000).
[35] B. Q. Sun, D. S. Jiang, X. D. Luo, Z. Y. Zu, Z. Pan, L. H. Li, and R. H. Wu, Appl. Phys. Lett. **76**, 2862 (2000).
[36] P. Krispin, S. G. Spruytte, J. S. Harris, and K. H. Ploog, J. Appl. Phys. **88**, 4153 (2000).
[37] P. Krispin, S. G. Spruytte, J. S. Harris, and K. H. Ploog, J. Appl. Phys. **90**, 2405 (2001).
[38] G. Duggan, J. Vac. Sci. Technol. B **3**, 1224 (1985).
[39] L. Bellaiche, S. H. Wei, and A. Zunger, Phys. Rev. B **56**, 10 233 (1997).
[40] E. P. O'Reilly, Semicond. Sci. Technol. **4**, 121 (1989).
[41] D. J. Wolford, J. A. Bradley, K. Fry and J. Thompson, in *Proceedings of the 17th Conference on the Physics of Semiconductors*, edited by J.D. Chadi and W. A Harrison(Springer, New York, 1985), p. 627.
[42] X. Liu, M. E. Pistol, L. Samuelson, S. Schwetlick, and W. Seifert, Appl. Phys. Lett. **56**, 1451 (1990).
[43] We justify set of parameters at the low temperature: $E_N = 1.65$ eV, $\beta = 2.45$ eV, and $E_g = 1.519$ eV, by comparing our theoretical prediction of lower conduction-band state E_- with those observed experimentally at the low temperature and reported by P. J. Klar *et al.*, Appl. Phys. Lett. **76**, 3439 (2000).
[44] M. R. Hofmann, N. Gerhardt, A. M. Wagner, C. Ellmers, F.

Höhnsdorf, J. Koch, W. Stolz, S. W. Koch, W. W. Rühle, J. Hader, J. V. Moloney, E. P. O'Reilly, B. Borchert, A. Y. Egorov, H. Riechert, H. C. Schneider, and W. W. Chow, IEEE J. Quantum Electron. **38**, 213 (2002).
[45] R. Fehse, S. Tomić, A. R. Adams, S. J. Sweeney, E. P. O'Reilly, A. Andreev, and H. Riechert, IEEE J. Sel. Top. Quantum Electron. **8**, 801 (2002).
[46] S. Tomić and E. P. O'Reilly, IEEE Photonics Technol. Lett. **15**, 6 (2003).
[47] P. N. Hai, W. M. Chen, A. Buyanova, H. P. Xin, and C. W. Tu, Appl. Phys. Lett. **77**, 1843 (2000).
[48] G. Baldassarri Höger von Högersthal, A. Polimeni, F. Masia, M. Bissiri, M. Capizzi, D. Gollub, M. Fischer, and A. Forchel, Phys. Rev. B **67**, 233304 (2003).
[49] F. Masia, A. Polimeni, G. Baldassarri Höger von Högersthal, M. Bissiri, M. Capizzi, P. J. Klar, and W. Stolz, Appl. Phys. Lett. **82**, 4474 (2003).
[50] R. J. Nicholas, in *Properties of III-V Quantum Wells and Superlattices*, edited by P. Bhattacharya (IEE INSPEC, London 1996), p. 75.
[51] P. R. C. Kent, L. Bellaiche, and A. Zunger, Semicond. Sci. Technol. **17**, 851 (2002).
[52] M. Hofmann, A. Wagner, C. Ellmers, C. Schlichenmeier, S. Schäfer, F. Höhnsdorf, J. Koch, W. Stolz, S. W. Koch, W. W. Rühle, J. Hader, J. V. Moloney, E. P. O'Reilly, B. Borchert, A. Y. Egorov, and H. Riechert, Appl. Phys. Lett. **78**, 3009 (2001).
[53] S. A. Choulis, T. J. C. Hosea, S. Tomić, M. Kamal-Saadi, A. R. Adams, E. P. O'Reilly, B. A. Weinstein, and P. J. Klar, Phys. Rev. B **66**, 165321 (2002).
[54] J. Wu, W. Shan, and W. Walukiewicz, Semicond. Sci. Technol. **17**, 860 (2002).
[55] A. Lindsay and E. P. O'Reilly (unpublished).
[56] I. Vurgaftman, J. R. Meyer, and L. R. Ram-Mohan, J. Appl. Phys. **89**, 5815 (2001).
[57] I. Vurgaftman and J. R. Meyer, J. Appl. Phys. **94**, 3675 (2003).